Individual A-Scan Signal Normalization Between Two Spectral Domain Optical Coherence Tomography Devices

Chieh-Li Chen,[1,2] Hiroshi Ishikawa,[1,2] Gadi Wollstein,[1] Yun Ling,[3] Richard A. Bilonick,[1,3] Larry Kagemann,[1,2] Ian A. Sigal,[1,2,4] and Joel S. Schuman[1,2,4]

[1]UPMC Eye Center, Eye and Ear Institute, Ophthalmology and Visual Science Research Center, Department of Ophthalmology, University of Pittsburgh School of Medicine, Pittsburgh, Pennsylvania
[2]Department of Bioengineering, Swanson School of Engineering, University of Pittsburgh, Pittsburgh, Pennsylvania
[3]Department of Biostatistics, Graduate School of Public Health, University of Pittsburgh, Pittsburgh, Pennsylvania
[4]McGowan Institute for Regenerative Science, University of Pittsburgh School of Medicine, Pittsburgh, Pennsylvania

Correspondence: Gadi Wollstein, UPMC Eye Center, Eye and Ear Institute, 203 Lothrop Street, Pittsburgh, PA 15213; wollsteing@upmc.edu.

C-LC and HI contributed equally to the work presented here and should therefore be regarded as equivalent authors.

Submitted: December 12, 2012
Accepted: April 16, 2013

Citation: Chen C-L, Ishikawa H, Wollstein, G, et al. Individual A-scan signal normalization between two spectral domain optical coherence tomography devices. *Invest Ophthalmol Vis Sci*. 2013;54:3463–3471. DOI:10.1167/iovs.12-11484

Purpose. We developed a method to normalize optical coherence tomography (OCT) signal profiles from two spectral-domain (SD) OCT devices so that the comparability between devices increases.

Methods. We scanned 21 eyes from 14 healthy and 7 glaucoma subjects with two SD-OCT devices on the same day, with equivalent cube scan patterns centered on the fovea (Cirrus HD-OCT and RTVue). Foveola positions were selected manually and used as the center for registration of the corresponding images. A-scan signals were sampled 1.8 mm from the foveola in the temporal, superior, nasal, and inferior quadrants. After oversampling and rescaling RTVue data along the Z-axis to match the corresponding Cirrus data format, speckle noise reduction and amplitude normalization were applied. For comparison between normalized A-scan profiles, mean absolute difference in amplitude in percentage was measured at each sampling point. As a reference, the mean absolute difference between two Cirrus scans on the same eye also was measured.

Results. The mean residual of the A-scan profile amplitude was reduced significantly after signal normalization (12.7% vs. 6.2%, $P < 0.0001$, paired *t*-test). All four quadrants also showed statistically significant reduction (all $P < 0.0001$). Mean absolute difference after normalization was smaller than the one between two Cirrus scans. No performance difference was detected between health and glaucomatous eyes.

Conclusions. The reported signal normalization method successfully reduced the A-scan profile differences between two SD-OCT devices. This signal normalization processing may improve the direct comparability of OCT image analysis and measurement on various devices.

Keywords: optical coherence tomography, image analysis, comparability

Optical coherence tomography (OCT) has been used widely and adopted as a standard of clinical care in ophthalmology for its ability to generate in vivo high-resolution cross-sectional images of the ocular tissues in a noninvasive and noncontact fashion.[1–3] OCT enables visualization and assessment of intraocular structures objectively and quantitatively, and helps identify the presence of disease and its progression.[4–7]

With recent introduction of spectral-domain (SD) OCT, multiple devices have been made available commercially from several different manufacturers. Each device is equipped with different light sources, acquisition speeds, and settings, providing a broad variety of options in terms of scan protocols, image processing, and presentation. However, this diversity results in OCT data incompatibility, like different scanning window sizes and data formats, and also causes OCT measurement data not to be comparable directly among different OCT devices.[8–14]

This incompatibility makes the visualization of OCT images machine-specific. OCT images obtained from different OCT devices must be displayed using different browsers and with different parameter settings. This adds complexity to clinical evaluation when browsing OCT images coming from different devices. Even with the image format standardization effort by the Digital Imaging and Communication in Medicine (DICOM),[15–17] different optical characteristics among various devices cannot be absorbed fully.

The systematic measurement differences among OCT devices poses a serious challenge in comparing OCT data measurements and influences the feasibility of including multiple OCT devices in the same study.[11–14] For a slow retinal damaged disease, like glaucoma, evaluation of the retinal nerve fiber layer (RNFL) thickness has an important role in the diagnosis and follow-up of the disease. However, if patients move from one clinic to another or device models from the same manufacturer change, the systematic differences between various OCT devices or between different device models result in the uselessness of the old data, and prevent us from establishing a long-term clinical record of RNFL thickness measurements. In addition, during multicenter clinical studies, OCT data coming from different clinical sites may be obtained with different OCT devices. The incompatibility between the

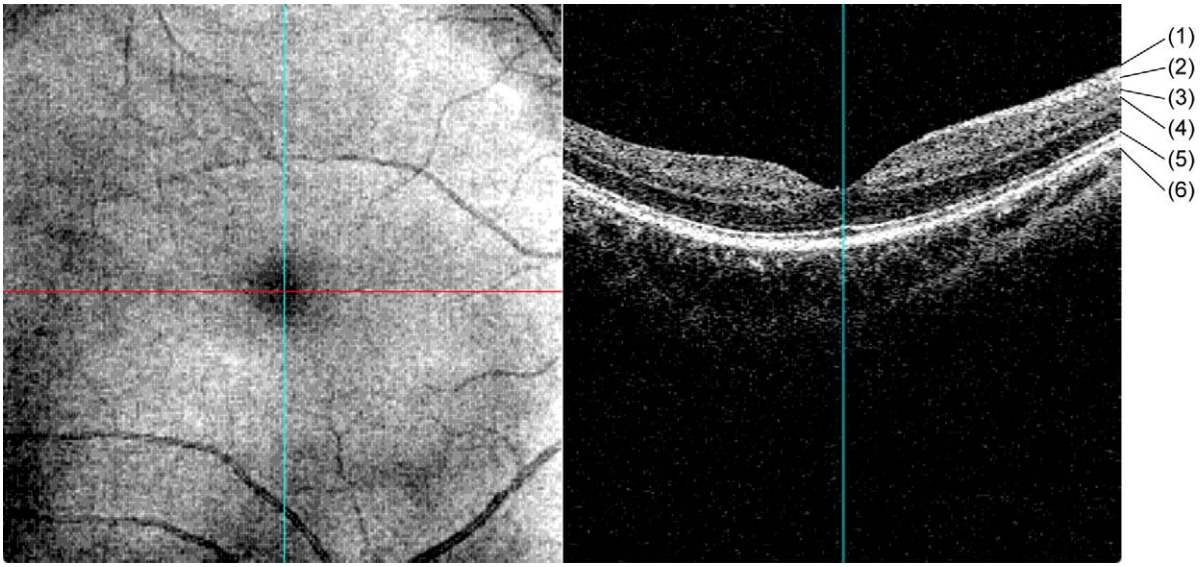

FIGURE 1. Foveola position was selected manually by looking for the largest separation between the junction of the IS and OS (**5**) of the photoreceptors and RPE (**6**). The *red line* on the en face image (*left*) indicates where the cross-sectional image on the *right* was sampled. The *vertical cyan line* indicates the location of the largest separation between the IS/OS of the photoreceptors and RPE. The intersection of the *red* and *cyan lines* on the en face image (*left*) is the selected foveola position. (**1**) Inner limiting membrane (ILM). (**2**) Nerve fiber layer (NFL). (**3**) Ganglion cell layer (GCL). (**4**) Inner platiform layer (IPL). (**5**) Inner and outer segments of the photoreceptors (IS/OS). (**6**) RPE.

measurement data would cause a serious problem in clinical practice and study design, and therefore a signal normalization algorithm, normalizing the various signal characteristics and reducing the systematic difference among different SD-OCT devices, is indispensible.

We hypothesized that the systematic difference in OCT measurements comes from the various signal characteristics among OCT devices and that the signal normalization method helps minimize the inherent OCT signal differences caused by optical characteristic variation among OCT machines. The purpose of our study was to develop and validate a method to normalize OCT signal profiles from two SD-OCT devices.

METHODS

Subjects

A total of 14 healthy and 7 glaucoma subjects volunteered to participate in this prospective cross-sectional study. One eye from each subject was selected randomly and used in the study. For the diseased eyes, a variety of glaucoma damage was included. The diagnosis of glaucoma was defined clinically based on the presence of visual field analysis and typical glaucomatous structural changes. All subjects were recruited at the University of Pittsburgh Medical Center Eye Center. The University of Pittsburgh Institutional Review Board and ethics committee approval were obtained for the study, and informed consent was obtained from all subjects. Our study followed the tenets of the Declaration of Helsinki, and was conducted in compliance with the Health Insurance Portability and Accountability Act.

Instruments and Image Acquisition

The macular region was imaged at the same visit using two commercially available SD-OCT devices with equivalent three-dimensional (3D) cube scan patterns: Cirrus HD-OCT (software version 5.1; Carl Zeiss Meditec, Inc., Dublin, CA) and RTVue (software version 6.1; Optovue, Inc., Fremont, CA).

Cirrus HD-OCT. Macular Cube 200 × 200 scan protocol was used to obtain the image data in our study. The scanning protocol collected 200 × 200 sampling points from a 6 × 6 mm^2 area centered on the foveola and 1024 samplings within a 2.00 mm axial scan depth.

RTVue OCT. A 200 × 200 raster cube scan protocol centered on the macula was used to obtain the image data in our study. We collected 200 × 200 sampling points from a 6 × 6 mm^2 area and 640 sampling points within a 1.96 mm axial scan depth in this scanning protocol.

For Cirrus and RTVue data, images with image quality below the manufacturer recommended cutoff, signal strength (SS) below 7 for Cirrus data, and signal strength index (SSI) below 40 for RTVue data, or images with apparent eye movement during scanning were considered poor quality images and discarded. Eye movement was defined subjectively as image artifacts on OCT en face (or OCT fundus) images showing a horizontal frame shift larger than one average size retinal blood vessel diameter and a major distortion of the fovea region.

All the image raw data were exported to a standalone computer for signal normalization and further analysis.

Signal Normalization

There were three stages of image processing: image registration and sampling, signal normalization, and A-scan profile comparison. For our study, we arbitrarily used the Cirrus OCT data format as a normalization reference, so the RTVue OCT data format was converted to a Cirrus-equivalent OCT data format.

Image Registration and Sampling. To sample the A-scan profile from the same location from different OCT data, the foveola position was selected manually on Cirrus and RTVue cube data by looking for the largest separation between the junction of the inner and outer segments (IS/OS) of the photoreceptors and RPE as appearing on the horizontal and vertical cross-sectional B-scans (Fig. 1). The selected foveola position then was used as the center for registration and sampling. RTVue data then were translated and rotated to match the blood vessel position subjectively on the Cirrus en

Investigative Ophthalmology & Visual Science

face image by finding the translation vector and rotation degree that minimizes the absolute differences in pixel value between Cirrus and RTVue en face images. After registration, single A-scans were sampled 1.8 mm from the foveola in the temporal, superior, nasal, and inferior quadrants from Cirrus and RTVue data, and were saved for further processing and analysis. The sampling position of each A-scan pair in Cirrus and RTVue was evaluated subjectively according to the relative position to major blood vessels. If the A-scan pairs were sampled from different positions in Cirrus and RTVue, the A-scan pairs were excluded. The flow of the preprocessing stage is shown in Figure 2.

Signal Normalization. The signal normalization consisted of three processing steps: z-scaling and sampling density normalization, speckle noise reduction, and amplitude normalization, and could be divided into two phases. In phase I, the effects of reducing the difference between Cirrus and RTVue of each processing step were assessed individually. In phase II, all three processing steps were combined together using different cutoffs and the final results were assessed.

The goal in phase I was to assess and optimize the ability to reduce the difference between Cirrus and RTVue OCT signals of each processing step. The testing started with z-scaling and sampling density normalization; after that, speckle noise reduction and amplitude normalization were applied separately as the second step, and the effects with various cutoffs were assessed. The details of each processing step are described below.

Z-Scaling and Sampling Density Normalization. In this step, the sampling densities in the axial direction between Cirrus and RTVue were matched. As mentioned above, Cirrus data has 1024 sampling points within a 2.00 mm scan depth, while RTVue data has 640 sampling points within a 1.96 mm scan depth. RTVue data were oversampled along the axial direction using bilinear interpolation to have the same sampling density as Cirrus OCT data. Sampling points locating beyond 1.96 mm scan depth were padded with the minimum value in the corresponding A-scan. After oversampling, RTVue was divided further by 16 to bring the 12-bit data format of RTVue to an 8-bit data format, so that RTVue and Cirrus data would be in a comparable intensity level. The z-scaling and sampling density normalized 8-bit RTVue data (Z-scaled RTVue data) then were used as the baseline RTVue data and further processing was performed on them.

Speckle Noise Reduction. After z-scaling and sampling density normalization, a speckle noise reduction method of our own design was applied to reduce the speckle noise. The algorithm was a localized high signal removing method. First, the heavily smoothed signal was generated based on the input signal. The intensity level of the smoothed signal was matched to the original one by mapping the low and high cutoffs after smoothing to the original ones; the outcome of this step then was used as a mask. Next, the high signal peaks outside the mask generated from the previous step were suppressed to the level of the mask, while the signals inside the mask were preserved. By this selective smoothing, high frequency components with relatively high amplitude were removed, while preserving high frequency components with low amplitude. Unlike many speckle reduction methods, instead of removing all the high frequency components regardless of the amplitude, this method preserved high frequency components with low amplitude and, therefore, more details of the tissue structures remained in the OCT signals after noise reduction. To test the effects of the various cutoff thresholds in the mask amplitude matching described above, the first, 33rd, 50th, and 66th percentiles on the histogram were used as the low cutoff. The high cutoff always was the 99th percentile.

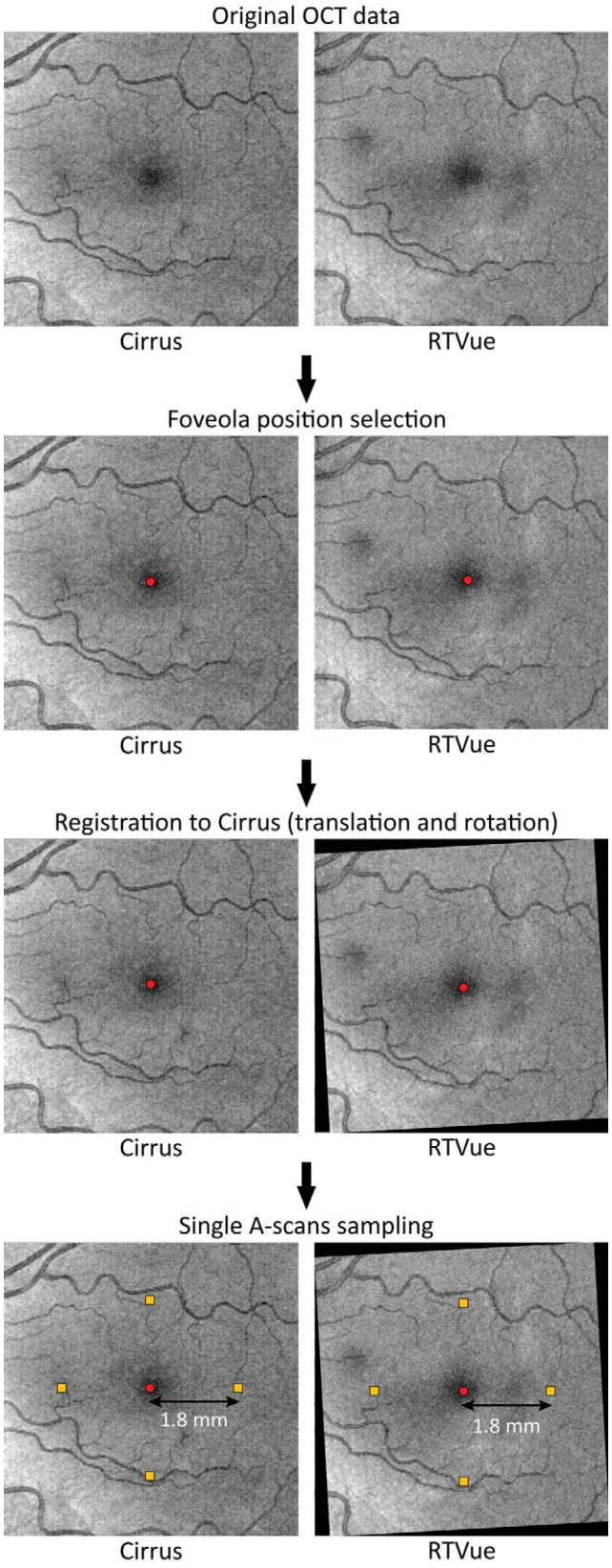

Figure 2. Image registration and sampling process: selecting foveola position, image registration, and single A-scan sampling.

Investigative Ophthalmology & Visual Science

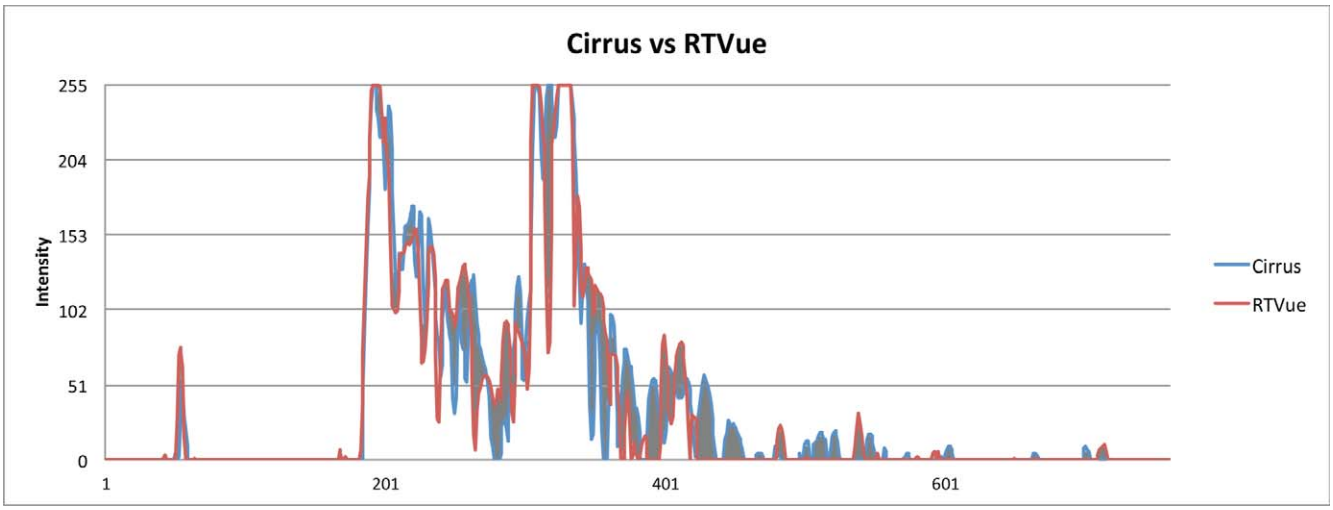

FIGURE 3. Absolute difference between final output of normalized Cirrus (*blue line*) and normalized RTVue (*red line*) A-scan profiles as recorded within the eligible measurement range. The *shaded area* between Cirrus and RTVue is the residual between the two A-scan profiles, and is used as a quantitative analysis parameter.

Amplitude Normalization. Amplitude normalization was designed to normalize the noise level between Cirrus and RTVue data. Various cutoffs were used for amplitude normalization to find the optimal settings: (1) A histogram-based amplitude normalization method was used here to map the signals linearly between low cutoffs (the first, 33rd, 50th, and 66th percentiles on the histogram of the frame where the sampled A-scan was located) and high cutoff (the 99th percentile on the histogram of the frame where the sampled A-scan was located) to the full 8-bit gray scale level on OCT data for Cirrus and RTVue; or (2) data range matching: matching the data range of two A-scan profiles by linearly mapping the minimal and maximal intensity value of the frame where the sampled A-scan was located to the full 8-bit gray scale for Cirrus and RTVue data.

In phase II, the three processing steps were combined and the outcomes of the combination of the three processing steps were evaluated. We combined the processing in the order that z-scaling and sampling density normalization came first, followed by speckle noise reduction, and then amplitude normalization with the cutoffs showing the best results in phase I.

A-Scan Profile Comparison. To assess the effects of the proposed algorithm, and the similarity of Cirrus and RTVue after signal normalization, each A-scan profile from Cirrus and RTVue sampled from the temporal, superior, nasal, and inferior quadrants was aligned to the inner limiting membrane (ILM), and the mean absolute difference in amplitude at each sampling point within the eligible measurement range was calculated after each processing step, where the eligible measurement range means that within this range, all the A-scan pairs were able to find corresponding Cirrus and RTVue data**.** Since original Cirrus and Z-scaled RTVue data had different data ranges compared to normalized Cirrus and RTVue data, the mean absolute difference in amplitude was normalized to the percentage of the maximal data range from the two A-scans to compensate the data range inconsistency, as shown in Equation 1. The absolute difference in amplitude between Cirrus and RTVue is presented as the shaded region between Cirrus and RTVue A-scan profiles (Fig. 3). The mean absolute difference in percentage between Cirrus and Z-scaled RTVue data was used as the baseline difference between the two OCT devices. Mean absolute difference in percentage between two Cirrus scans, acquired from the same eye at the same visit sampled at the same location, was computed and used as the reference for similarity assessment. The same eligible measurement range was applied to calculate the mean absolute difference in percentage between two Cirrus scans.

$$\text{Mean absolute difference } (\%) = \frac{\sum_i \left(\frac{|Cirrus_i - RTVue_i|}{Max\ Data\ Range} \right)}{Eligible\ Measurement\ Range} \times 100\% \quad (1)$$

Statistical Analysis

Paired *t*-tests were used to analyze the overall and quadrant absolute differences between original Cirrus and Z-scaled RTVue data, between normalized Cirrus and normalized RTVue data, and between two original Cirrus scans. $P < 0.05$ was considered as statistically significant.

RESULTS

Subject demographics are presented in Table 1. We enrolled 14 healthy and 7 glaucoma subjects in our study. Healthy eyes were younger than glaucomatous eyes (41.9 ± 16.9 vs. 65.2 ± 5.5 years, $P = 0.0023$, *t*-test).

Table 2 summarizes the mean absolute difference in amplitude in percentage of A-scan profiles between original Cirrus and Z-scaled RTVue data (baseline residual), and between Cirrus and RTVue data after speckle noise reduction with various cutoff settings. The differences of baseline residual from the residual after speckle noise reduction were shown in parentheses. The minus sign indicates that there was a reduction in the residual between Cirrus and RTVue after speckle noise reduction. The overall residual was statistically significantly reduced after speckle noise reduction with the settings using the 33rd percentile on the histogram as the low

TABLE 1. Subject Demographics

	Healthy, $n = 14$	Glaucoma, $n = 7$
Male/female	4:10	1:6
OD/OS	10:4	4:3
Age, y	41.9 ± 16.9	65.2 ± 5.5
MD	0.6 ± 0.6	−2.0 ± 2.0
Total retinal thickness	303.8 ± 12.5	297.8 ± 8.2

Investigative Ophthalmology & Visual Science

Table 2. Mean Absolute Difference in Amplitude Between Cirrus and RTVue A-Scan Profiles Using Speckle Noise Reduction as the Next Step Following Z-Scaling and Sampling Density Normalization

	Overall (%)	Temporal (%)	Superior (%)	Nasal (%)	Inferior (%)
Baseline residual	12.7	12.8	12.4	13.0	12.6
First percentile	14.6 (1.9)	15.9 (3.1)	13.3 (0.9)	15.5 (2.5)	13.7 (1.1)
33rd percentile	12.4 (−0.3)	12.7 (−0.1)	12.1 (−0.2)	12.6 (−0.5)	12.3 (−0.3)
50th percentile	12.7 (−0.0)	13.0 (0.3)	12.4 (0.1)	12.8 (−0.2)	12.5 (−0.0)
66th percentile	12.8 (0.1)	13.1 (0.3)	12.6 (0.2)	12.9 (−0.1)	12.6 (−0.0)

Absolute difference is in percentage with the difference of baseline residual from the residual after speckle noise reduction in parentheses.

cutoff and the 99th percentile as the high cutoff ($P = 0.0031$, paired *t*-test), but not when using the 50th and 66th percentile on the histogram as the low cutoff. When using the first percentile on the histogram as the low cutoff, the residual was significantly increased ($P < 0.0001$, paired *t*-test). Among all the settings, using the 33rd percentile on the histogram as the low cutoff statistically significantly outperformed the settings with the rest low cutoffs ($P < 0.0001$), and generated the largest reduction in residual in amplitude between Cirrus and RTVue. For quadrant analysis, only the superior quadrant with the 33rd percentile on the histogram as the low cutoff showed a statistically significant reduction compared to the baseline residual. For the 50th and 66th percentile on the histogram as the low cutoffs, there was no significant difference in residual compared to baseline in all four quadrants. When using the first percentile on the histogram as the low cutoff, the residuals significantly increased in all the quadrants. A similar trend as the overall results was found in the quadrants analysis that using the 33rd percentile on the histogram as the low cutoff statistically significantly reduced the baseline residual most compared to other settings ($P < 0.0048$).

Table 3 shows the mean absolute difference in amplitude in percentage of A-scan profiles between original Cirrus and Z-scaled RTVue data (baseline residual), and between Cirrus and RTVue data with amplitude normalization as the second step after z-scaling and sampling density normalization using various cutoff settings. The differences of baseline residual from the residual after amplitude normalization were shown in parentheses. The minus sign indicates that there was a reduction in the residual between Cirrus and RTVue after amplitude normalization. The overall residual was statistically significantly reduced when using the 50th and 66th percentile on the histogram as the low cutoff and the 99th percentile on the histogram as the high cutoff (both $P < 0.0001$, paired *t*-test). No significant difference in the residual before and after amplitude normalization was found when using the 33rd percentile on the histogram as the low cutoff. A statistically significant increase in the residual was detected when applying the first percentile on the histogram as the low cutoff and using the data range matching method (both $P < 0.0001$, paired *t*-test). Among the settings that successfully reduced the residual, the method using histogram-based amplitude normalization with the 66th percentile as the low cutoff statistically significantly outperformed other settings and contributed to the largest amount of reduction compared to baseline residual. For the quadrant analysis, the same trends as the overall results were found in all four quadrants.

In phase II, for the combined signal normalization method, the three processing steps were combined in the following order: z-scaling and sampling density normalization followed by speckle noise reduction, and at the end of signal normalization, we performed amplitude normalization. The settings that generated the best results of each processing step were used in the final combined method. For the speckle noise reduction step, the 33rd and 99th percentile on the histogram were used as the low and high cutoff. In amplitude normalization, the histogram-based amplitude normalization method with the 66th and 99th percentiles on the histogram as the low and high cutoffs was used to remove the noise level difference, and match the different data range between Cirrus and RTVue.

An example of step-by-step signal normalization in phase II is presented in Figure 4. The first row in Figure 4 shows the original A-scan profile from two SD-OCT devices, with Cirrus in blue and RTVue in red. For display purposes, the dynamic range of RTVue data was rescaled linearly from 12-bit to 8-bit gray scale in Figure 4 (the first row). A-scan profiles from Cirrus and RTVue were aligned to ILM, so the effect of signal normalization can be appreciated easier. As the first row in Figure 4 shows, the original A-scan profiles looked dissimilar, and had different noise levels and sampling densities. The second row in Figure 4 presents the results after z-scaling and sampling density normalization. After oversampling RTVue data in the axial direction, the sampling density of the two A-scan profiles became the same and the peaks in the A-scan profiles matched. However, there still is a noise level difference between Cirrus and Z-scaled RTVue data. The third row in Figure 4 shows the results after speckle noise reduction. Compared to the second row, the high spiky peaks were removed, and at the same time, the high frequency components with low intensity values were kept intact. The last row in Figure 4 shows the final results. After amplitude normalization, the noise level of the two A-scan profiles became the same and the A-scan profiles looked similar.

Table 3. Mean Absolute Difference in Amplitude Between A-Scan Profiles Using Amplitude Normalization as the Next Step Following Z-Scaling and Sampling Density Normalization

	Overall (%)	Temporal (%)	Superior (%)	Nasal (%)	Inferior (%)
Baseline residual	12.7	12.8	12.4	13.0	12.6
First percentile	20.5 (7.8)	20.8 (8.0)	20.2 (7.9)	20.8 (7.8)	20.0 (7.4)
33rd percentile	12.6 (−0.0)	12.6 (−0.1)	12.4 (0.0)	12.9 (−0.1)	12.5 (−0.1)
50th percentile	10.7 (−2.0)	10.6 (−2.2)	10.5 (−1.9)	11.0 (−2.0)	10.6 (−2.0)
66th percentile	8.7 (−4.0)	8.6 (−4.2)	8.5 (−3.9)	9.1 (−3.9)	8.6 (−4.0)
Data range matching	19.6 (6.9)	20.3 (7.5)	18.9 (6.5)	19.8 (6.8)	19.4 (6.8)

Absolute difference is in percentage with the difference of baseline residual from the residual after amplitude normalization in parentheses.

Investigative Ophthalmology & Visual Science

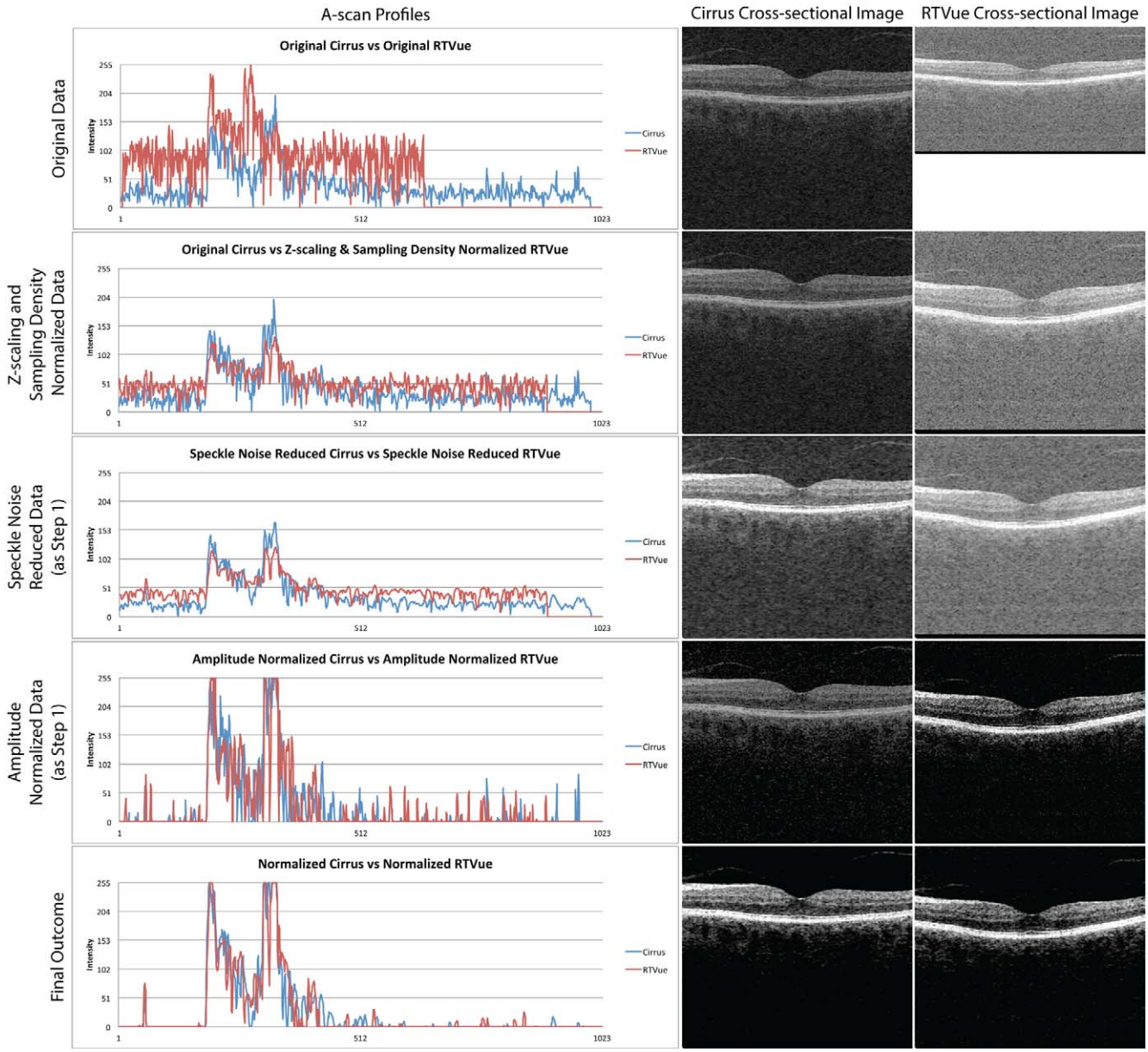

Figure 4. Profiles of signal intensity at the level of the inner limiting membrane per pixel in the consecutive steps of the signal normalization procedure. *First row*: original A-scan profiles from Cirrus (*blue*) and RTVue (*red*). For display purposes, the A-scan profile from RTVue was scaled linearly from 12-bit to 8-bit. *Second row*: after amplitude normalization, the distance between noise levels from Cirrus and RTVue equals zero. *Third row*: speckle noise reduction. *Last row*: z-scaling and sampling density normalization. Signal profiles of the devices become similar at the end of the process.

Table 4 summarizes the mean absolute amplitude differences in percentage between two A-scan profiles from two Cirrus scans, from Cirrus and Z-scaled RTVue scans, from normalized Cirrus and RTVue scans, and from two normalized Cirrus scans. Two A-scan pairs in the temporal quadrant, 2 A-scan pairs in the superior quadrant, 1 A-scan pair in the nasal quadrant, and 2 A-scan pairs in the inferior quadrant were excluded because of misalignment. The mean absolute difference in percentage between Cirrus and RTVue was statistically significantly reduced after signal normalization (12.7% vs. 6.2%, $P < 0.0001$, paired *t*-test). The mean absolute difference in amplitude in percentage between Cirrus and RTVue also was statistically significantly decreased after normalization in all quadrants ($P < 0.0001$, paired *t*-test).

After signal normalization, the overall mean absolute difference in percentage between Cirrus and RTVue was statistically significantly smaller compared to the difference between two Cirrus scans (6.2% vs. 9.9%, $P < 0.0001$, paired *t*-test), indicating that the signal normalization process successfully reduced the differences, even lower than the level of the intradevice difference. Similar results were found in quadrant analysis, the difference between Cirrus and RTVue was statistically significantly smaller compared to the difference between two Cirrus scans in all four quadrants ($P < 0.0001$, paired *t*-test).

The last row in Table 4 summarizes the residual in percentage between two normalized Cirrus scans. After signal normalization, the residual in percentage between two scans from the same device also was statistically significantly reduced for mean and all quadrants ($P < 0.0001$ for all comparisons, paired *t*-test), indicating that the proposed signal normalization method also worked on the OCT data obtained using the same

Investigative Ophthalmology & Visual Science

Table 4. Mean Absolute Difference in Amplitude Between A-Scan Profiles

	Overall % (95% CI)	Temporal, $n = 19$ (95% CI)	Superior, $n = 19$ (95% CI)	Nasal, $n = 20$ (95% CI)	Inferior, $n = 19$ (95% CI)
Original Cirrus vs. original Cirrus	9.9 (9.6, 10.1)	10.0 (9.4, 10.5)	9.9 (9.3, 10.6)	9.6 (9.2, 10.0)	9.9 (9.4, 10.4)
Original Cirrus vs. Z-scaled RTVue	12.7 (12.4, 13.0)	12.8 (12.1, 13.4)	12.4 (11.6, 13.1)	13.0 (12.5, 13.5)	12.6 (12.0, 13.2)
Normalized Cirrus vs. normalized RTVue	6.2 (6.0, 6.4)	6.0 (5.6, 6.4)	6.2 (5.8, 6.7)	6.5 (6.2, 6.9)	6.2 (5.8, 6.5)
Normalized Cirrus vs. normalized Cirrus	6.0 (5.8, 6.2)	5.9 (5.3, 6.5)	6.2 (5.7, 6.7)	5.9 (5.6, 6.2)	6.0 (5.6, 6.3)

Absolute difference is in percentage with 95% confidence interval (CI) in parentheses.

device. Comparing the residual between normalized Cirrus and RTVue, and two normalized Cirrus data, the overall residual was statistically significantly different (6.3% vs. 6.0%, $P = 0.03$, paired *t*-test). For the quadrant analysis, there was no statistically significant difference in the residual between two normalized comparison pairs except for the nasal quadrant ($P = 0.0006$).

Tables 5 and 6 present the results divided by the clinical grouping. Statistically significant reduction in the mean absolute difference in percentage between Cirrus and RTVue after signal normalization was observed for healthy and glaucoma groups for mean and all quadrants ($P < 0.0147$, paired *t*-test). Furthermore, after signal normalization, the absolute difference in percentage between Cirrus and RTVue also was statistically significantly smaller compared to the difference between two Cirrus scans in all comparisons for each group.

Discussion

A novel signal normalization method was developed to reduce the A-scan profile differences between two SD-OCT devices in our study. The presented method successfully reduced the differences between A-scan profiles from Cirrus and RTVue.

The effect on reducing the residual (in percentage) between Cirrus and RTVue A-scan profiles of speckle noise reduction and amplitude normalization was assessed separately. Each processing step focused on different factors that result in the dissimilarity between Cirrus and RTVue signals, and solved them from a different aspect. Speckle noise reduction was applied to eliminate the differences between Cirrus and RTVue A-scan profiles caused by the randomly distributed high spiky signal (considered as the speckle noise). Amplitude normalization was designed to remove the noise level difference between two devices. Overall, both processing steps significantly reduced the A-scan profile residual with some tested cutoffs. Nevertheless, since each individual processing step focused on one particular factor, the ability to reduce the residual between Cirrus and RTVue of each one was limited. These 2 processing steps are complementary to each other to achieve the optimized signal normalization.

The optimized cutoff settings for each processing step were different, indicating that the cutoff settings were processing specific. Various cutoffs were used and tested for their ability to reduce the residual between Cirrus and RTVue in speckle noise reduction and amplitude normalization. Different reactions to reduce the residual with various cutoffs were observed between individual processing steps. To optimize the signal normalization method, the cutoffs that showed the best results were chosen when combining each processing step to build the final signal normalization method. For speckle noise reduction, the 33rd percentile on the histogram was picked; and for amplitude normalization, the 66th percentile on the histogram was used as the low cutoff to remove the noise level difference. There still is some room for further optimization of the method, like systematic software training with feedback to find the optimal solution. Further investigation is warranted.

We picked the 66th percentile on the histogram as the low cutoff for amplitude normalization as the best setting. Though setting an even higher cutoff for amplitude normalization may have provided smaller residuals, we needed to strike a balance between reducing the profile differences and preserving the actual retinal signals. Based on the statistical analysis of the regular retinal thickness of the entire scan length of the OCT frame, the meaningful retinal signals form approximately one-third of the OCT images. The same analysis results also are applied in traditional and conventional ways of displaying OCT images on the devices using false-color scheme; lower 66% of signals (or similar cutoff) usually are considered as noise signals and removed, and the entire OCT images are rescaled further so that the detail of retinal tissues can be appreciated in a clearer way for physicians to make clinical diagnoses.

Despite the fact that our results support and work well with the notion of using the 66th percentile as the low cutoff, there still is possibility that we may discard some actual retinal tissue signal having intensity weaker than the strong noise signal by cutting off low intensity pixels, which may lose important information from ocular tissues. To calculate dynamically the optimized cutoff for multiple SD-OCT devices that separates true tissue signal from the noise, Huang et al. have developed a method based on histogram density modeling and decomposition.[18] However, they found that the overlap of weak retinal tissue signal and strong noise signal is relatively wide, and results in the limitation that we may lose information from retinal tissues having less reflectivity by cutting off low intensity pixels. Further improvement on this issue is required.

One of the advantages of the proposed algorithm is the use of the selective smoothing in the speckle noise reduction method. Speckle noise, inherently existing in all OCT images and causing

Table 5. Mean Absolute Difference in Amplitude Between A-Scan Profiles for Clinical Groups, Healthy Subjects ($n = 14$)

	Overall % (95% CI)	Temporal, $n = 13$ (95% CI)	Superior, $n = 12$ (95% CI)	Nasal, $n = 14$ (95% CI)	Inferior, $n = 14$ (95% CI)
Original Cirrus vs. original Cirrus	9.7 (9.5, 10.0)	9.7 (9.1, 10.2)	9.9 (9.2, 10.6)	9.5 (9.0, 10.0)	9.9 (9.3, 10.5)
Original Cirrus vs. Z-scaled RTVue	12.6 (12.3, 13.0)	12.7 (11.8, 13.6)	12.3 (11.4, 13.2)	13.0 (12.3, 13.6)	12.5 (11.8, 13.2)
Normalized Cirrus vs. normalized RTVue	6.3 (6.1, 6.5)	6.1 (5.5, 6.7)	6.3 (5.8, 6.9)	6.5 (6.0, 7.0)	6.1 (5.7, 6.6)
Normalized Cirrus vs. normalized Cirrus	6.0 (5.8, 6.2)	5.9 (5.3, 6.4)	6.3 (5.6, 7.0)	5.9 (5.5, 6.2)	6.0 (5.6, 6.4)

Absolute difference is in percentage with 95% CI in parentheses.

Investigative Ophthalmology & Visual Science

Table 6. Mean Absolute Difference in Amplitude Between A-Scan Profiles for Clinical Groups, Glaucoma Subjects ($n = 7$)

	Overall % (95% CI)	Temporal, $n = 6$ (95% CI)	Superior, $n = 7$ (95% CI)	Nasal, $n = 6$ (95% CI)	Inferior, $n = 5$ (95% CI)
Original Cirrus vs. original Cirrus	10.1 (9.6, 10.6)	10.6 (9.1, 12.1)	10.0 (8.5, 11.5)	9.9 (9.1, 10.6)	9.9 (8.8, 10.9)
Original Cirrus vs. Z-scaled RTVue	12.9 (12.3, 13.4)	13.0 (12.1, 14.0)	12.4 (10.9, 14.0)	13.2 (11.9, 14.4)	12.8 (11.6, 14.1)
Normalized Cirrus vs. normalized RTVue	6.1 (5.8, 6.5)	5.8 (4.9, 6.7)	6.0 (5.1, 7.0)	6.5 (5.7, 7.3)	6.2 (5.5, 6.9)
Normalized Cirrus vs. normalized Cirrus	6.0 (5.6, 6.4)	6.0 (4.3, 7.7)	6.0 (5.0, 7.0)	6.0 (5.3, 6.7)	5.9 (5.0, 6.9)

Absolute difference is in percentage with 95% CI in parentheses.

the granular appearance of OCT images, degrades the quality of the images and influences the performance of image data analysis. Unlike other noise reduction methods, which remove the speckle noise, but also blur the fine-textured regions resulting in lower apparent resolution in the final output OCT images, our speckle noise reduction method selectively removes the high peaks' signals (speckle noise) while preserving the high frequency components with low amplitude signals. In this way, the speckle noise reduced signal maintains enough details in the low and medium intensity range.

Another advantage of the proposed method is the combination of multiple image-processing techniques (z-scaling and sampling density normalization, speckle noise reduction, and amplitude normalization) into one fully automated algorithm to overcome all factors contributing to the systematic difference between various OCT devices. This approach is population-independent; does not require training or tuning parameters, or converting equations for different OCT devices or cohorts; and can be applied to any OCT device. This would allow establishing a common standard for OCT image data so universal visualization and analysis software can handle any OCT data independent of device specific differences.

The proposed signal normalization method can be applied to and works for all sampling points in the cube data. However, for validation purposes, the sampling location was chosen to have all the inner retinal layers distinguishable, as the layers merge or disappear in the area close to the foveola, while avoiding the major retinal blood vessels (Fig. 1). It is known that blood vessels reflect and block the light signal, which causes shadowing artifacts that obscure the ocular tissue information beyond the blood vessels (Fig. 5).[19,20]

The reasons for successful normalization using 8-bit data format as the standard data format can be explained from three aspects. Current display systems are using 8-bit data format for display purposes; therefore, even though we have a higher dynamic range, such as 12-bit or 16-bit data format, down-sampling of the OCT data is needed for display, which might degrade the image quality. For image processing performance, a majority of the image processing techniques used in computer vision or computer graphics focuses on 8-bit data format images, and it has been proved that 8-bit data format is sufficient to provide satisfactory and reliable processing and segmentation results.[21] Finally, data size is smaller by converting OCT data to 8-bit data format, which would save memory space, and accelerate the processing time of image analysis and data transfer.

Other intensity profile normalization methods of OCT images across different eyes using the same devices have been developed to compensate the RNFL thickness measurement variability caused by inconsistent attenuation of the reflectivity between healthy and diseased eyes, and to increase the sensitivity and specificity of disease detection.[22,23] Many studies solved the A-scan profile intensity variation by normalizing the RNFL signal intensity to the brightest layer in the OCT image, usually the RPE, as a preprocessing step before thickness measurement to reduce the variation. Those methods are simple and easy to implement, and can be applied to the entire OCT image. However, they require a robust segmentation algorithm to detect accurately the positions and

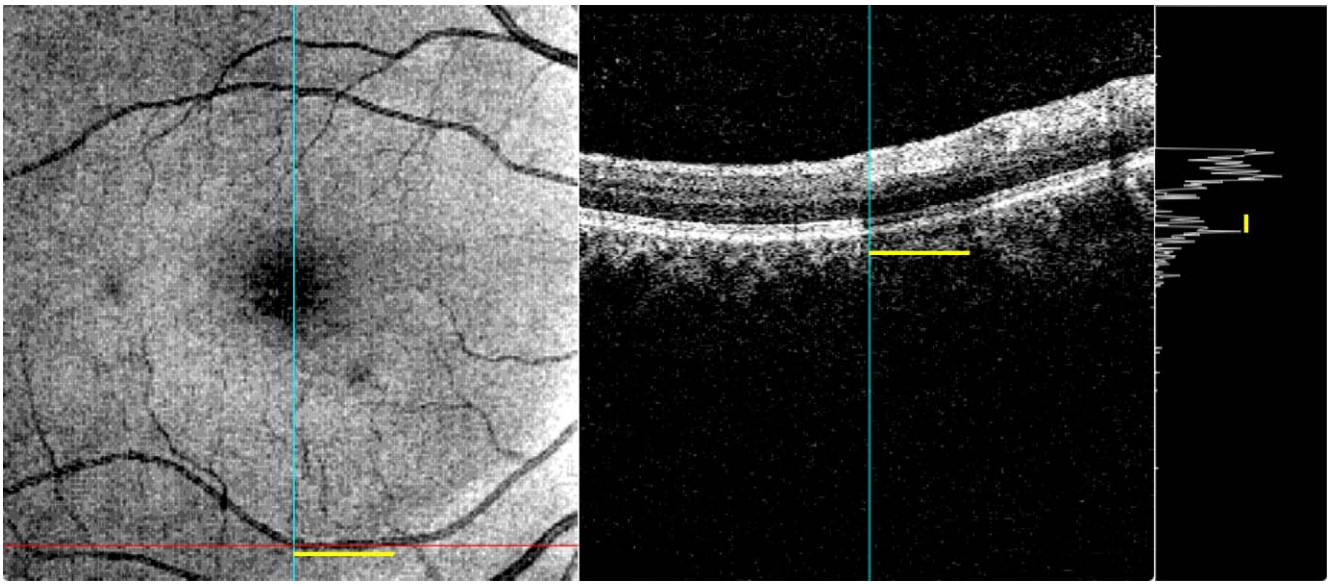

Figure 5. Shadow effect of blood vessel on OCT image quality and signal strength. The *horizontal red line* on the en face image (*left*) indicates the position where the cross-sectional image (*middle*) was sampled, 2.61 mm away from the foveola. A dramatic drop of the signal strength can be observed at the positions where blood vessel lies (the *yellow bar*) on the cross-sectional image (*middle*) and the A-scan profile (*left*), which is sampled from the position of the *cyan vertical line*.

boundaries of RNFL and RPE, which can be a challenge especially with coexisting retinal pathology. Another disadvantage of those methods is the assumption that the relative signal intensity of adjacent retinal layers is the same across different eyes and SD-OCT devices. From our observation, A-scan profiles varied substantially among different eyes and SD-OCT devices. Even on the same eye, on different devices, they can differ significantly from each other on the intensity proportions among various retinal sub-layers. For example, A-scan profiles from Cirrus and RTVue (the second row of Fig. 4) have different contrast between high and low intensity signal, where the contrast is larger in Cirrus than in RTVue, which results in different responses from the same segmentation algorithm, or different RNFL thickness measurements. In contrast, our method does not require any segmentation before the normalization and has no assumption about the intensity profiles being similar on the same eye across different devices. In addition, our signal normalization works equally well on healthy and glaucomatous eyes, indicating that the proposed method is capable of compensating signal characteristic differences independent from the pathologic state, where the RNFL signals generally are weaker and show somewhat different A-scan profiles.

Although we only tested the effect of the method with Cirrus and RTVue devices, in principle, this normalization method can be applied to all SD-OCT devices. Further investigation is warranted.

In conclusion, the reported novel signal normalization method successfully reduced the A-scan profile differences between Cirrus and RTVue SD-OCT in healthy and glaucomatous eyes. This signal normalization method would allow establishing fundamental signal compatibility among multiple OCT devices, which would make the analysis and measurement results from various devices directly comparable.

Acknowledgments

Presented in part at the annual meeting of the Association for Research in Vision and Ophthalmology, Fort Lauderdale, Florida, May 2012.

Supported in part by National Institutes of Health Contracts R01-EY013178, R01 EY011289, P30 EY008098 (Bethesda, Maryland); The Eye and Ear Foundation (Pittsburgh, Pennsylvania); and unrestricted grants from Research to Prevent Blindness (New York, New York).

Disclosure: **C.-L. Chen**, None; **H. Ishikawa**, None; **G. Wollstein**, Allergan (C); **Y. Ling**, None; **R.A. Bilonick**, None; **L. Kagemann**, None; **I.A. Sigal**, None; **J.S. Schuman**, P

References

1. Drexler W, Fujimoto JG. State-of-the-art retinal optical coherence tomography. *Prog Retin Eye Res*. 2008;27:45–88.
2. Gabriele ML, Wollstein G, Ishikawa H, et al. Three dimensional optical coherence tomography imaging: advantages and advances. *Prog Retin Eye Res*. 2010;29:556–79.
3. Gabriele ML, Wollstein G, Ishikawa H, et al. Optical coherence tomography: history, current status, and laboratory work. *Invest Ophthalmol Vis Sci*. 2011;52:2425–36.
4. Hee MR, Izatt JA, Swanson EA, et al. Optical coherence tomography of the human retina. *Arch Ophthalmol*. 1995;113:325–332.
5. Schuman JS, Hee MR, Arya AV, et al. Optical coherence tomography: a new tool for glaucoma diagnosis. *Curr Opin Ophthalmol*. 1995;6:89–95.
6. Schuman JS, Hee MR, Puliafito CA, et al. Quantification of nerve fiber layer thickness in normal and glaucomatous eyes using optical coherence tomography. *Arch Ophthalmol*. 1995;113:586–96.
7. Schuman JS, Pedut-Kloizman T, Hertzmark E, et al. Reproducibility of nerve fiber layer thickness measurements using optical coherence tomography. *Ophthalmology*. 1996;103:1889–1898.
8. Sung KR, Kim DY, Park SB, et al. Comparison of retinal nerve fiber layer thickness measured by Cirrus HD and Stratus optical coherence tomography. *Ophthalmology*. 2009;116:1264–1270.
9. Knight OJ, Chang RT, Feuer WJ, et al. Comparison of retinal nerve fiber layer measurements using time domain and spectral domain optical coherent tomography. *Ophthalmology*. 2009;116:1271–1277.
10. Vizzeri G, Weinreb RN, Gonzalez-Garcia AO, et al. Agreement between spectral-domain and time-domain OCT for measuring RNFL thickness. *Br J Ophthalmol*. 2009;93:775–781.
11. Leite MT, Rao HL, Weinreb RN, et al. Agreement among spectral-domain optical coherence tomography instruments for assessing retinal nerve fiber layer thickness. *Am J Ophthalmol*. 2011;151:85–92.
12. Kanamori A, Nakamura M, Tomioka M, et al. Agreement among three types of spectral-domain optical coherent tomography instruments in measuring parapapillary retinal nerve fibre layer thickness. *Br J Ophthalmol*. 2012;96:832–837.
13. Tan BB, Natividad M, Chua KC, et al. Comparison of retinal nerve fiber layer measurement between 2 spectral domain OCT instruments. *J Glaucoma*. 2012;21:266–273.
14. Buchser NM, Wollstein G, Ishikawa H, et al. Comparison of retinal nerve fiber layer thickness measurement bias and imprecision across three spectral-domain optical coherence tomography devices. *Invest Ophthalmol Vis Sci*. 2012;53:3742–3747.
15. DICOM Standards Committee. Proposal for collaboration between DICOM and the International Working Group for intracoronary OCT standardization and validation (IWG-OCT). Available at: http://medical.nema.org/dicom/minutes/committee/2009/2009-04-21/other_documents/wg-01_proposed%20collaboration_iwg-oct.doc Accessed September 4, 2012.
16. Sihan K, Botha C, Post F, et al. Fully automatic three-dimensional quantitative analysis of intracoronary optical coherence tomography: method and validation. *Cathet Cardiovasc Intervent*. 2009;74:1058–1065.
17. Chiang MF, Boland MV, Brewer A, et al. Special requirements for electronic health record systems in ophthalmology. *Ophthalmology*. 2011;118:1681–1687.
18. Huang Y, Gangaputra S, Lee KE, et al. Signal quality assessment of retinal optical coherence tomography images. *Invest Ophthalmol Vis Sci*. 2013;53:2133–2141.
19. Fabritius T, Makita S, Hong Y, et al. Automated retinal shadow compensation of optical coherence tomography images. *J Biomed Opt*. 2009;14:010503.
20. Girard MJA, Strouthidis NG, Ethier CR, et al. Shadow removal and contrast enhancement in optical coherence tomography images of the human optic nerve head. *Invest Ophthalmol Vis Sci*. 2011;52:7738–7748.
21. Tappeiner C, Barthelmes D, Abegg MH, et al. Impact of optic media opacities and image compression on quantitative analysis of optical coherence tomography. *Invest Ophthalmol Vis Sci*. 2008;49:1609–1614.
22. van der Schoot J, Vermeer KA, de Boer JF, et al. The effect of glaucoma on the optical attenuation coefficient of the retinal nerve fiber layer in spectral domain optical coherence tomography images. *Invest Ophthalmol Vis Sci*. 2012;53:2424–2430.
23. Vermeer KA, van der Schoot J, Lemij HG, et al. RPE-normalized RNFL attenuation coefficient maps derived from volumetric OCT imaging for glaucoma assessment. *Invest Ophthalmol Vis Sci*. 2012;53:6102–6108.

Investigative Ophthalmology & Visual Science